IEEE Access
Multidisciplinary | Rapid Review | Open Access Journal

Received 31 August 2023, accepted 4 October 2023, date of publication 11 October 2023, date of current version 18 October 2023.

Digital Object Identifier 10.1109/ACCESS.2023.3323593

RESEARCH ARTICLE

A Comparison of PCA and LBF Based Multireceiver SAS Imaging Algorithms

MENG WANG AND PAN HUANG, (Member, IEEE)
School of Mathematics and Information Science, Weifang University, Weifang 261061, China

Corresponding author: Pan Huang (wfxyhp@wfu.edu.cn)

This work was supported in part by the Natural Science Foundation of Shandong Province under Grant ZR2023MD122, and in part by the Doctoral Fund of Weifang University under Grant 2019BS04.

ABSTRACT Multireceiver synthetic aperture sonar (SAS) is a useful tool to provide high-resolution images. The most important step lies in developments of multireceiver synthetic aperture image formation processors, which uses the sonar echoed signal as the input. The system transfer function is crucial in the development of signal processors. In order to use traditional imaging algorithms, the monostatic conversion transferring multireceiver SAS signal to monostatic SAS data is often conducted. A review and evaluation of imaging methods based on monostatic conversion is conducted in this article. The relationship of Phase center approximation (PCA) method and Loffeld's bistatic formula (LBF) is firstly reformulated in theory. Considering facts that PCA and LBF methods are the approximation of exact system transfer function, the approximation error of both methods are firstly compared and evaluated by using the numerical system transfer function, which is considered to be the precise system transfer function. Since more approximations of PCA and LBF should be carried out to develop fast imaging algorithms, the actual phase error of both methods is compared and evaluated based on numerical system transfer function. Then, the imaging performance of both methods based on range migration algorithm (RMA) is further evaluated. At last, the relationships of both patent methods are comprehensively described.

INDEX TERMS Synthetic aperture sonar, imaging processor, system transfer function, phase center approximation, Loffeld's bistatic formula, phase error, imaging performance.

I. INTRODUCTION

Synthetic aperture sonar (SAS) [1], [2], [3], [4], [5], [6], [7] is a high-resolution equipment which can provide high quality images of seafloor [8], [9], [10], [11], [12]. With this tool, the users can easily find small objects such as pipeline and so on in seafloor. Besides, using a high-resolution image [13], [14], [15], [16], object recognition [17], [18], [19], [20], [21] can be performed quickly.

For synthetic aperture sonar, the most important step is to process raw echoed signal, which is highly based on the matched filtering [22], [23], [24]. The multireceiver SAS system made up of a single transmitter and many receivers can be decomposed into many bistatic SAS systems, and the mapping rate can be highly improved compared to traditional monostatic SAS. Traditional imaging techniques rely mostly on a monostatic SAS system. At this point, traditional imaging methods are unable to be used directly to a multireceiver SAS system. A simple processing idea is to transfer multireceiver SAS signal to monostatic SAS data. Traditional imaging techniques can then be used directly to process transferred datasets. The phase center approximation (PCA) [25], [26], [27], [28] and Loffeld's bistatic formula (LBF) [29], [30], [31], [32], [33], [34] can cope with the data transferring. The PCA approach assumes a virtual sensor is situated in the middle position of each transmitter/receiver sub-system. Consequently, each bistatic sonar is replaced by the virtual sensor, and monostatic equivalent datasets can be obtained. However, this method would suffer from approximation error [35], [36]. On the one hand, the error named PCA error [36], [37], [38], [39] is generated by this approximation operation. On the other hand, another error

The associate editor coordinating the review of this manuscript and approving it for publication was Xuebo Zhang.

which is hard to be considered by this method would result from the stop-and-hop approximation. Aiming to correct the PCA error [37], the range difference between the exact slant range and approximated range based on PCA methodology is deduced [40]. To compensate the stop-and-hop error [41], [42], the propagation time of reference target at the center of mapping swath [43] is used. To some degree, the approximation error is partly compensated by using both methods. However, there is still residual error. With the method in [44], both errors are well considered by using the quadratic expansion like Taylor approximation. Unfortunately, the variation of the approximate azimuth error is not taken into account. When the high-quality SAS system is used, this will result in image distortion. Based on the relationship between azimuth Doppler and instantaneous angle [28], this problem is well solved, and the datasets of high-resolution SAS system can also be well focused. LBF [30], [45], [46], [47], [48] is another method which can transfer the multireceiver SAS signal to monostatic SAS datasets. With the LBF, both the transducer and hydrophone contribute equally to the azimuth Doppler. Then, the points of stationary phase matching to the transducer and hydrophone phases are found by employing the method of stationary phase. The transducer phase and hydrophone phase are approximated by quadratic-Taylor approximation, and the common point of stationary phase is got. Consequently, the spectrum is obtained. Like the transfer function of PCA method, the transfer function of LBF can also be decomposed into two parts. One term is identical to the typical monostatic SAS system's system transfer function, while the other is heavily dependent on the finite aperture between transducer and hydrophone. After compensating the baseline dependent term, the SAS signal from several receivers can be translated to monostatic SAS datasets. In order to correct the baseline dependent term's range variance, the range sub-block processor is provided. There are two blockwise approaches. With the first one, the datasets should be segmented into several sub-blocks at first, and then the compensation is conducted in the spectrum domain for each blockwise data [30]. Based on the other one [49], the whole datasets are directly compensated in the 2D frequency domain, and then the range blockwise related to the compensation function is extracted. Compared to the first sub-block processing method, the second approach can avoid the convolution error at the edge of each sub-block. In general, both sub-block processing methods can well obtain the monostatic equivalent SAS data.

Both PCA method and LBF can carry out the monostatic conversion from different views. The main contributions and innovations of this paper are summarized as follows.

(1) The PCA and LBF methods are proposed in SAS and synthetic aperture radar (SAR) fields [50], [51], [52], and their relationships are nearly neglected. With our paper, the inherent relationships of PCA and LBF methods are comprehensively discussed by analyzing their spectrums. Both methods are mostly identical from the spectrum view. The spectrum analysis and error analysis further enhance this conclusion.

(2) Traditional SAS/SAR imaging algorithms just focus on the phase error of spectrum as it is the key to develop Fourier-domain imaging algorithms. In practice, further approximations with respect to the spectrum should be performed before developing imagery algorithms. In this paper, the actual phase error is proposed to quantitatively evaluate these approximations. That is to say, the PCA and LBF methods are not identical from the view of actual phase error.

(3) The computation load of both methods is compared in detail, and the LBF method is much more efficient compared to PCA method.

In this paper, the echo model is displayed in section II. In section III, the PCA and LBF are simply recalled. In section IV, the relationships between PCA and LBF methods are comprehensively discussed. After that, the simulations are used to find out which approach is optimum. In the final section, several conclusions are formed.

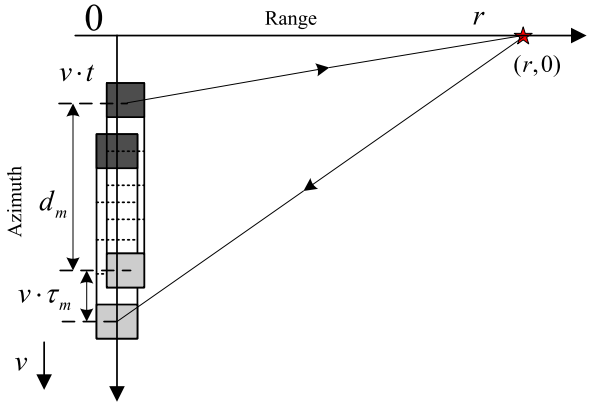

FIGURE 1. Multireceiver SAS imaging geometry.

II. ECHO SIGNAL MODEL

Fig. 1 displays the collecting model of SAS system.

The black sensor represents the transducer, while additional ones are M receivers that comprise a receiver array. The array would moves in azimuth. The coordinates of a point-like scatterer is $(r, 0)$. The hyperbolic distance between transmitter and target is calculated by the transmitter location in the azimuth dimension, and it is

$$R_T = \sqrt{r^2 + (vt)^2} \tag{1}$$

The variable t represents the azimuth slow time. Taking into account receiver movement during signal transmission, the hyperbolic range between the mth hydrophone and scatterer is

$$R_{Rm} = \sqrt{r^2 + (vt + d_m + 2v \cdot r/c)^2} \tag{2}$$

The variable d_m is the baseline aperture between the transducer and the mth hydrophone.

The symbol v stands for the sonar velocity. When the chirp is emitted, the received waveform [53], [54], [55] of the mth hydrophone is shown as

$$ss_m(\tau, t) = p\left(\tau - \frac{R_T + R_{Rm}}{c}\right) \cdot \exp\left\{-\mathrm{j}2\pi f_c \frac{R_T + R_{Rm}}{c}\right\} \tag{3}$$

In (3), $p(\tau)$ is the emitted chirp signal. τ shows the range fast time. f_c stands for the waveform carrier. c denotes the acoustic wave velocity.

III. TWO METHODS DESCRIPTIONS

This section simply recalls PCA and LBF methods at first.

A. PCA METHODS

By introducing a virtual transducer in the middle position of each bistatic SAS system [26], [27], [56], the equivalent slant range $R_m(t; r)$ is shows

$$R_m(t; r) \approx 2\sqrt{r^2 + (vt + v\frac{r}{c} + \frac{d_m}{2})^2} + \frac{(v\frac{2r}{c} + d_m)^2}{4r} \tag{4}$$

Applying the method of stationary phase, the point of stationary phase can be obtained. Then, the spectrum is further got, and it shows

$$\begin{aligned}\varphi_m(f_\tau, f_t; r) = &\underbrace{-4\pi\frac{r}{c}\sqrt{(f_c + f_\tau)^2 - \frac{c^2 f_t^2}{4v^2}}}_{\text{Monostatic term}} \\ &+ \underbrace{2\pi f_t \frac{r}{c}}_{\text{Azimuth shifting term}} + \underbrace{\pi f_t \frac{d_m}{v}}_{\text{Bistatic term}} \\ &\underbrace{- \pi (f_c + f_\tau)\frac{\left(2\frac{v}{c}r + d_m\right)^2}{2rc}}_{\text{Bistatic error}}\end{aligned} \tag{5}$$

In (5), the spectrum of emitted waveform is neglected. The Doppler and instantaneous frequencies are f_t, f_τ, individually. In (5), the monostatic phase is close to that of traditional one. The second term in (5) is the azimuth shifting, which is caused by approximation error. The third term in (5) is generated by bistatic SAS sampling. The last term in (5) stands for the approximation phase caused by PCA and stop-and-hop approximation operations.

B. LBF METHODS

The contribution to Doppler by transducer and hydrophone are the same for LBF approach [30], [31], [32], [33]. At this point, the points of stationary phase corresponding to transducer and hydrophone phase histories can be obtained, individually. Then, the quadratic expansion of transducer and hydrophone phase histories are carried out, separately. The method of stationary phase is further used to obtain the common point of stationary phase. The spectrum is expressed as

$$\begin{aligned}\theta_m(f_\tau, f_t; r) = &\underbrace{-4\pi\frac{r}{c}\sqrt{(f_c + f_\tau)^2 - \frac{c^2 f_t^2}{4v^2}}}_{\text{Monostatic term}} \\ &+ \underbrace{2\pi f_t \frac{r}{c}}_{\text{Azimuth shifting term}} + \underbrace{\pi f_t \frac{d_m}{v}}_{\text{Bistatic term}} \\ &\underbrace{- \frac{\pi}{c}\frac{\left(d_m + \frac{2rv}{c}\right)^2}{(f_c + f_\tau)^2}\frac{\left[(f_c + f_\tau)^2 - \frac{f_t^2 c^2}{4v^2}\right]^{3/2}}{2r}}_{\text{Bistatic error}}\end{aligned} \tag{6}$$

The monostatic term in (6) is still equivalent to that of traditional system. The next term in (6) stands for the azimuth shifting, which is caused by approximation error. The third term in (6) is the bistatic phase produced by bistatic SAS sampling. The last term in (6) denotes the approximation error caused by LBF method.

IV. RELATIONSHIPS DISCUSSIONS

In this section, the relationships between both methods are analyzed in theory. After that, the phase errors with both methods in theory and practice are discussed in detail.

A. RELATIONSHIPS BETWEEN LBF AND PCA

By comparing Eq. (5) and Eq. (6), both final terms are where we find the major difference. The azimuth Doppler is given by

$$f_t = \frac{f_c + f_\tau}{c} 2v \sin\vartheta \tag{7}$$

The variable in Eq. (7) shows the angle between instantaneous position of sonar and target. In practice, the squint angle ϑ is within $\pm 10°$. That is to say, the Doppler frequency f_t is sometimes few tens Hertz while the center frequency f_c and instantaneous frequency f_τ are few tens of kilohertz. At this point, we can obtain the following inequality.

$$\left(\frac{cf_t}{2v}\right)^2 \ll (f_c + f_\tau)^2 \tag{8}$$

Based on (8), the last term in (6) is reformulated as

$$\begin{aligned}&\frac{\pi}{c}\frac{\left(d_m + \frac{2rv}{c}\right)^2}{(f_c + f_\tau)^2}\frac{\left[(f_c + f_\tau)^2 - \frac{f_t^2 c^2}{4v^2}\right]^{3/2}}{2r} \\ &\approx \frac{\pi}{c}\frac{\left(d_m + \frac{2rv}{c}\right)^2}{(f_c + f_\tau)^2}\frac{\left[(f_c + f_\tau)^2\right]^{3/2}}{2r} \\ &= \frac{\pi (f_c + f_\tau)\left(d_m + \frac{2rv}{c}\right)^2}{2cr}\end{aligned} \tag{9}$$

Inspecting (9) and the last term in Eq. (5), we find that both terms are equally consistent with each other.

TABLE 1. The high frequency system.

SAS Parameters	Value	Units
waveform carrier	150000	Hz
emitted waveform bandwidth	15000	Hz
SAS moving velocity	150	cm/s
receiver azimuth size	4	cm
receiver array size	120	cm
transmitter azimuth size	8	cm
pulse repetition interval	400	ms

B. PHASE ERROR IN THEORY

The PCA and LBF methods are the approximations of accurate spectrum. At this point, the phase error in theory is mainly discussed in this section. Since the accurate spectrum is not analytically obtained, the numerical spectrum is used as the benchmark, and the phase of numerical spectrum for each bistatic SAS system is denoted as Θ_m [11]. Therefore, the approximation errors of PCA and LBF methods are denoted by

$$\Delta\varphi_m(f_\tau, f_t; r) = \Theta_m - \varphi_m \tag{10}$$

$$\Delta\theta_m(f_\tau, f_t; r) = \Theta_m - \theta_m \tag{11}$$

Inspecting Eq. (10) and Eq. (11), we discover that the approximation error is greatly dependent on the four factors including the range, Doppler and instantaneous frequencies, together with finite aperture between transducer and hydrophone. We can talk about the phase error for each bistatic SAS system to make the analysis simpler. In general, when the largest instantaneous frequency is employed, the maximum error magnitude is realized. At this point, the phase error versus with instantaneous frequency is not discussed here.

1) PHASE ERROR WITH HIGH FREQUENCY SAS SYSTEM

The phase errors with high and low center frequencies cases are discussed. Firstly, we go through high frequency SAS system phase error. The parameters in Table 1 are displayed.

We compute the phase error for the first and last bistatic SAS systems. With the first bistatic SAS system, the transducer and hydrophone are quite close. With the last bistatic SAS system, the transducer and hydrophone are far apart. The phase errors of first and last bistatic SAS systems are displayed in Fig. 2 and Fig. 3, individually.

It is should be noted that the close range used in this section is 45 m while the far range is 280 m. From Fig. 2 and Fig. 3, we easily observe from a comparison of Figures 2 and 3 that the phase errors of the two methods are nearly identical. That is to say, both methods are nearly equivalent to each other when the high frequency SAS system is used. This is entirely consistent with the findings made in section III-B.

2) PHASE ERROR WITH LOW FREQUENCY SAS SYSTEM

We focus on phase error for low frequency SAS systems in this section. The low frequency system is presented in Table 2.

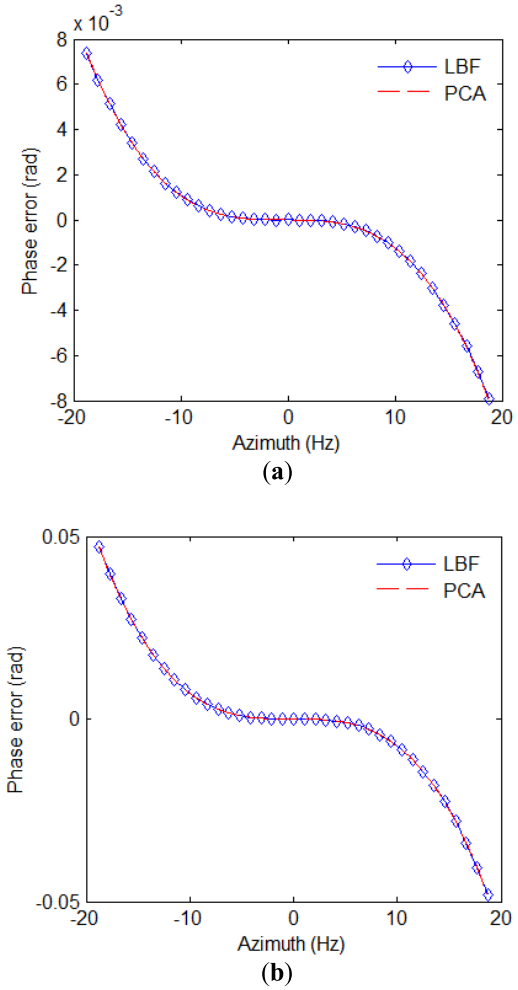

FIGURE 2. Phase error of the first bistatic SAS system for high frequency SAS. (a) close range; (b) far range.

TABLE 2. The low frequency system.

SAS Parameters	Value	Units
waveform carrier	60000	Hz
emitted waveform bandwidth	15000	kHz
SAS moving velocity	150	cm/s
receiver azimuth size	4	cm
receiver array size	120	cm
transmitter azimuth size	8	cm
pulse repetition interval	400	ms

The phase errors of the first and last bistatic SAS systems are depicted in Figs. 4 and 5, individually, when the SAS system operates at low frequency. The close range used in this section is still 45 m while the far range is 280 m. From Fig. 4, when the transmitter and receiver are close to one another, both systems continue to produce the same phase errors. The phase error in Fig. 5 exhibits a little difference at close range when the receiver and transmitter are far apart. In general, the error difference at close range can be neglected. Both

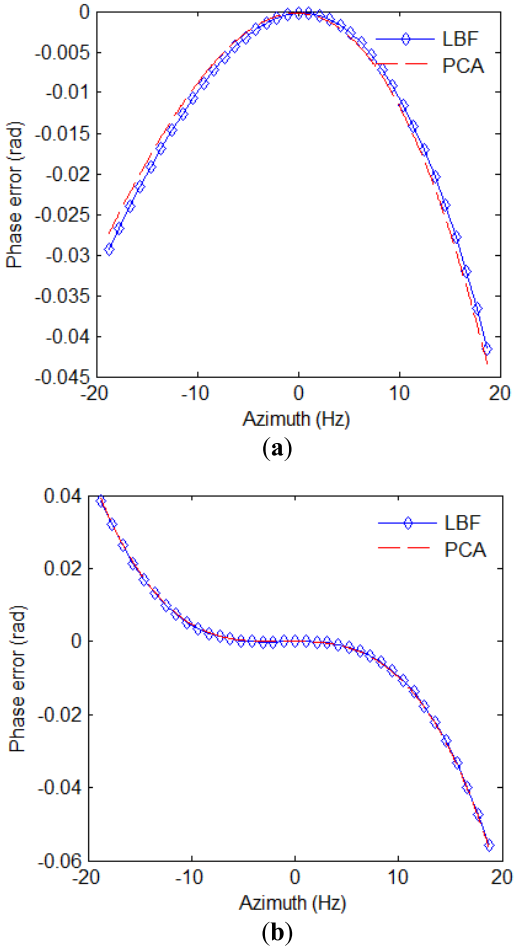

FIGURE 3. Phase error of the last bistatic SAS system for high frequency SAS. (a) close range; (b) far range.

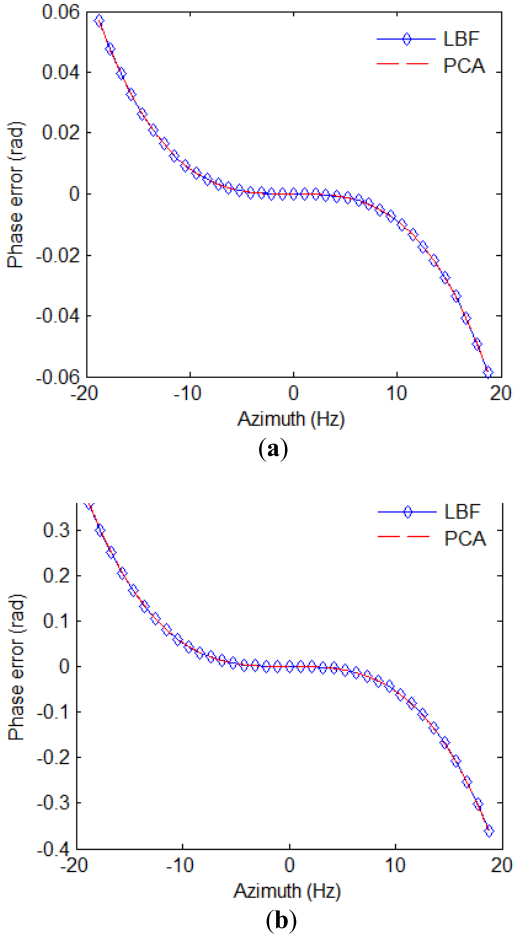

FIGURE 4. Phase error of the first bistatic SAS system for low frequency SAS. (a) close range; (b) far range.

approaches' phase errors remain the same when the target is positioned at far distances. It is important to remember that the phase inaccuracy in the low frequency situation is greater than the high frequency one. The reason behind this is that the synthetic aperture time is longer than that with high frequency case. As both methods do not take into account the error compensation of azimuth variance, the phase error slightly increases with Doppler frequency.

Summarily, the phase errors of PCA and LBF methods are nearly identical with low frequency case. Based on section III.D, we draw a conclusion that the LBF and PCA methods are identical. This conclusion is in line with the one found in section III-A.

C. ACTUAL PHASE ERROR

Eq. (5) and Eq. (6) are the point target response spectrum, which is also called system transfer function. Both spectrums are computed for a single target in imaging area. Due to the space variance of approximation error, the spectrums shown in Eq. (5) and Eq.(6) cannot be directly applied to develop imaging algorithms. In order to handle this problem, more operations with respect to approximation error in Eq. (5) and Eq. (6) should be carried out. These operations would bring another phase errors. This paragraph will talk about the actual phase inaccuracy from an imaging perspective. This section continues to use the simulation parameters from section III-B.

1) ACTUAL PHASE ERROR WITH PCA METHOD

Inspecting the approximation error in Eq. (5), we find that the instantaneous frequency and range can be decoupled in fast time domain. In other words, the approximation range error based on Eq. (5) is represented by the following formula.

$$\Delta_{PCA,m}(r) = \frac{\left(2\frac{v}{c}r + d_m\right)^2}{4rc} \tag{12}$$

This error is range variant for each bistatic SAS system. The interpolation can be easily exploited to correct the approximation error. Here, we neglect the error introduced by interpolation. The actual phase error of the PCA approach is still the same with the phase error in theory because no change with respect to Eq. (10) is used. That is to say, the phase error of PCA method in section III-B is also the actual phase error of PCA method.

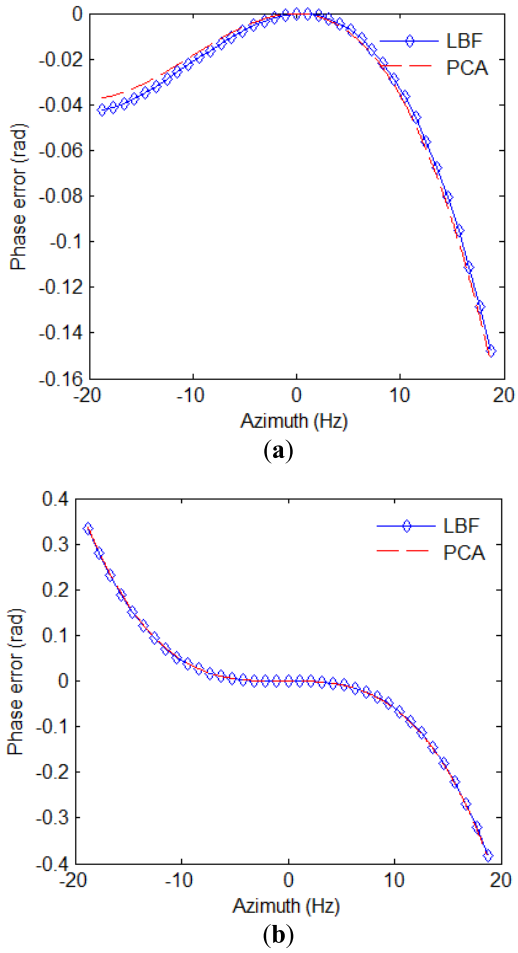

FIGURE 5. Phase error of the last bistatic SAS system for low frequency SAS. (a) close range; (b) far range.

2) ACTUAL PHASE ERROR WITH LBF METHOD

Inspecting the approximation error shown in Eq. (6), we discover that the approximation error relies on the baseline aperture between the transducer and hydrophone, the Doppler frequency, the instantaneous frequency, and the range. More importantly, the coupling of approximation error between instantaneous frequency and range cannot be decoupled. Currently, the interpolation used by PCA method cannot be used to eliminate the approximation error of the LBF approach. The straightforward compensation technique is based on the range blockwise approach. It means that the datasets are segmented into sub-blocks in range. Then, the approximation error of the LBF method at the reference range is utilized as the compensation function to account for the error over the entire sub-block. The error for targets positioned in reference range is entirely corrected. However, the residual phase errors would affect focusing quality of targets which are outside of the reference range. In general, the sub-block processing would bring further phase error. Consequently, the actual phase error of LBF is no longer the phase error showed in III.B. Summarily, the residual error increases with sub-block width. To simplify the analysis, the optimum sub-block width which is about 10 m is used in this section. For simplicity, the last term in Eq. (6) is rewritten as

$$\Delta\phi_{LBF,m}(f_\tau, f_t; r) = \frac{\pi}{c}\frac{\left(d_m + \frac{2rv}{c}\right)^2}{(f_c + f_\tau)^2}\frac{\left[(f_c + f_\tau)^2 - \frac{f_t^2 c^2}{4v^2}\right]^{3/2}}{2r} \tag{13}$$

Then, the actual phase error is shown as

$$\Delta\varphi_m(f_\tau, f_t; r) = \Theta_m - \big(\varphi_m + \Delta\phi_{LBF,m}(f_\tau, f_t; r) - \Delta\phi_{LBF,m}(f_\tau, f_t; r_{ref})\big) \tag{14}$$

r_{ref} in Eq. (14) denotes the distance of reference target, which is often the center target in each sub-block. From Eq. (14), the actual phase error of LBF is identical to phase error in theory at reference range. However, when the target is outside the range of reference, the actual phase error would increase.

3) ACTUAL PHASE ERROR ANALYSIS

Figs. 6-Fig. 9 display the actual phase errors based on SAS systems in section III-B. These phase errors allow us to deduce three key findings. Firstly, when transmitter/receiver baseline distance grows, the actual phase error of LBF also does. Fig. 6(a) and Fig. 8(a) enhance this conclusion. Secondly, the actual phase error of LBF at far range is close to the error of PCA technique. The reason behind this is that the quadratic expansion is used by LBF. With this approximation, the large error is produced at close range while the minor error is generated at far range. The phase errors shown in Fig. 6- Fig. 9 strength this conclusion. Thirdly, the actual phase error of LBF slightly depends on frequency. When the high frequency is used, the actual error at close range is large. However, the actual error is slight. Fig. 7(a) and Fig. 9(a) further validate this conclusion. The reason lies in that the actual phase error of high frequency SAS system is much more sensitive to that with low frequency SAS system.

V. COMPARISON OF COMPUTATION LOAD

The main focus of this section is the computation burden [57] with the compensation of bistatic error in Eq. (5) and (6). The interpolation process is the primary component of error correction for the PCA method. For clarity, N_r stands for the total amount of collecting data in range. N_a stands for the total amount of collecting data in azimuth. N_interp is the interpolation kernel length. The interpolation computation burden is $\mathrm{O}(2N_\mathrm{interp} - 1)$. Considering PCA technique, the computation burden of error correction is

$$O_{PCA} = \left(2N_\mathrm{interp} - 1\right) N_r \times N_a \tag{15}$$

For FT or IFT operations, the computation burden is $\mathrm{O}(1.5N_\mathrm{r}\log_2 N_\mathrm{r})$ for N_r sampling points. For LBF method, the sub-block approach is utilized to cope with the bistatic error. With each sub-block, the multiplication and FT/IFT are mainly exploited. We suppose that within the sub-block with N sampling point is generated in the range dimension.

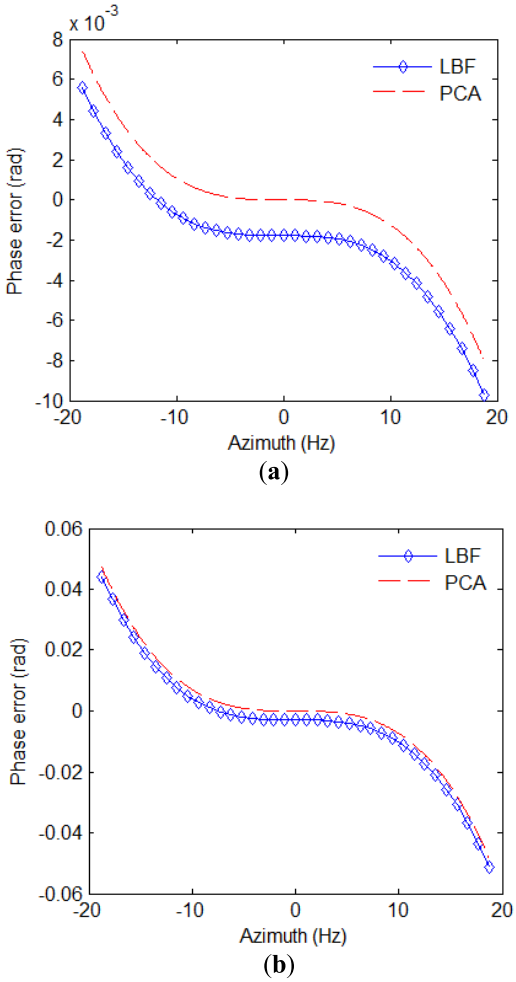

FIGURE 6. Actual phase error of the first bistatic SAS system for high frequency SAS. (a) close range; (b) far range.

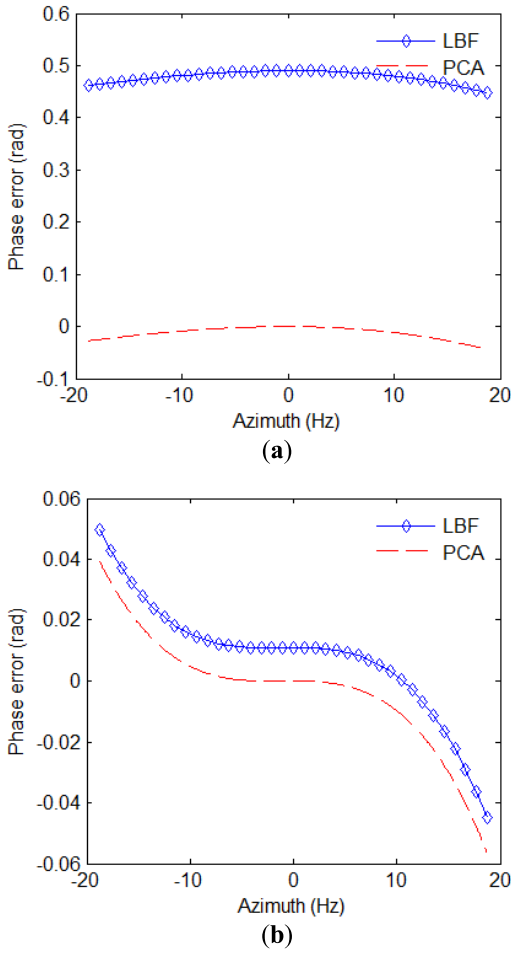

FIGURE 7. Actual phase error of the last bistatic SAS system for high frequency SAS. (a) close range; (b) far range.

Considering LBF technique, the computation burden of error compensation is

$$O_{LBF} = 3MN \log_2 N + N_a \times N \tag{16}$$

Comparing Eq. (15) and Eq. (16), our research shows that the LBF method is more effective than the PCA method.

VI. SIMULATIONS

Simulations are performed in this section to further validate the conclusions stated in section III. We continue to employ the simulation parameters specified in Section III. Here, the range migration algorithm [58], [59], [60], [61], [62] is used in this section.

A. HIGH FREQUENCY CASE

The imaging results of the PCA approach for the high frequency case are given in Fig. 10. At close range, we discover that the imaging result of PCA is superior to that of LBF. Both approaches can achieve comparable image performance at far range.

The slices of azimuth quality are displayed in Fig. 11 to compare imaging capability. We find that the focusing performance of LBF method suffers from deterioration compared to that of PCA method. The reason behind this is that the high-resolution SAS system suffers from large actual phase error at close range, which is discussed in section III.C. Inspecting Fig. 11(b), the imaging performance based on PCA and LBF methods are mostly identical at far range. The conclusions are well consistent with results drawn from section III.

The performance of both methods is compared from the view of peak sidelobe level ratio (PSLR), integrated sidelobe level ratio (ISLR) and azimuth resolution (AR), which are showed in Table 3. Based on Table 3, the PSLR and ISLR of LBF method is lower than PSLR and ISLR of PCA method at close range. The phase error of PCA method can be well compensated while that of LBF method is compensated by blockwise method, which would lead to residual phase error for target not at reference range. Therefore, the focusing of close target is seriously affected. When the target is at far range, the focusing quality is nearly the same with PCA method. These conclusions also agree with reports from section IV-B and IV-C.

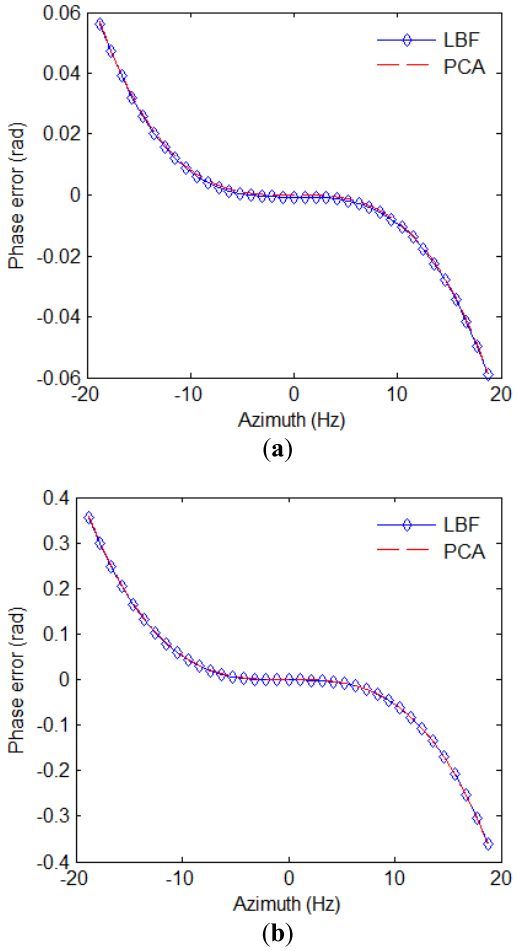

FIGURE 8. Actual phase error of the first bistatic SAS system for low frequency SAS. (a) close range; (b) far range.

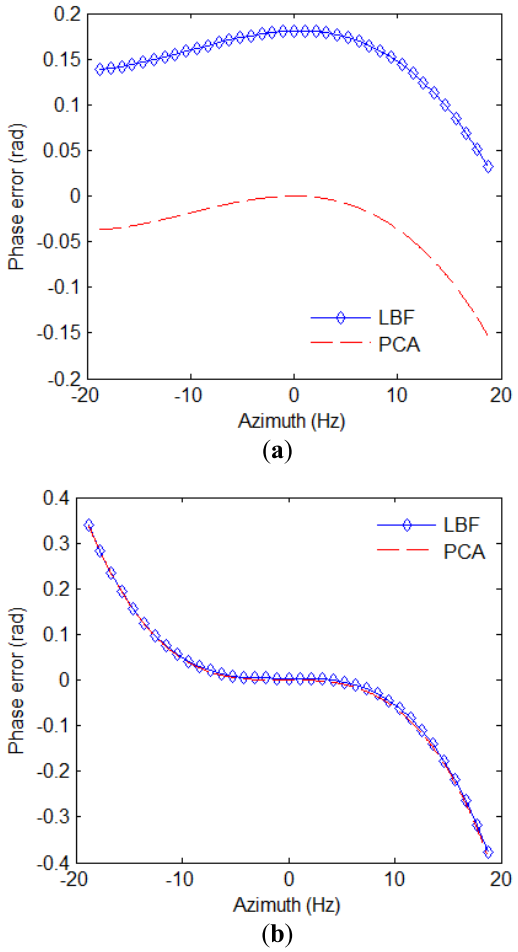

FIGURE 9. Actual phase error of the last bistatic SAS system for low frequency SAS. (a) close range; (b) far range.

TABLE 3. Performance of high frequency system.

	Close target			Far target		
	PSLR(dB)	ISLR(dB)	AR(cm)	PSLR(dB)	ISLR(dB)	AR(cm)
PCA	-14.70	-9.40	4	-14.77	-10.26	4
LBF	-14.32	-8.24	4	-14.77	-10.26	4

B. LOW FREQUENCY CASE

The focusing data and azimuth slices for the low frequency situation are presented in Figs. 12 and 13, respectively.

From Fig. 12 and Fig. 13, we find that the focusing result of LBF is inferior to that of PCA at close range. Comparing imaging results of high and low frequency SAS systems, the imaging result of low frequency SAS at close range is superior to that of high frequency SAS at far range. This finding is accordance with that of III.C.

The performance of both methods is compared from the view of peak sidelobe level ratio (PSLR), integrated sidelobe level ratio (ISLR) and azimuth resolution (AR), which are shown in Table 4. From Table 4, the performance of LBF method is still lower than that of PCA method at close range. For far target, the performance of both methods is nearly identical. This is still the same with conclusion based on section IV.

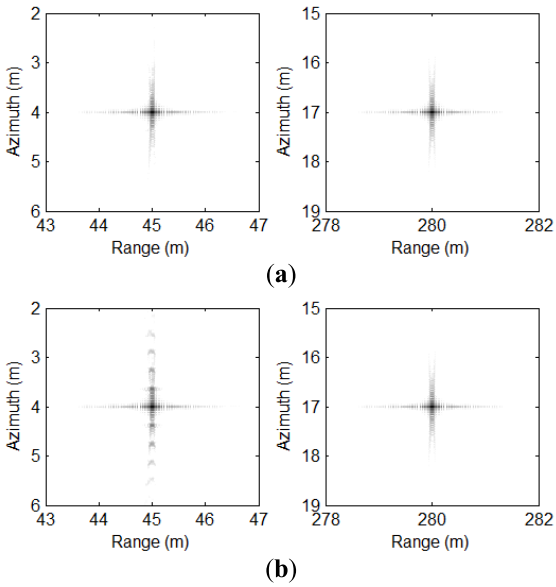

FIGURE 10. Imaging results of PCA method for high frequency SAS. (a) PCA method; (b) LBF method.

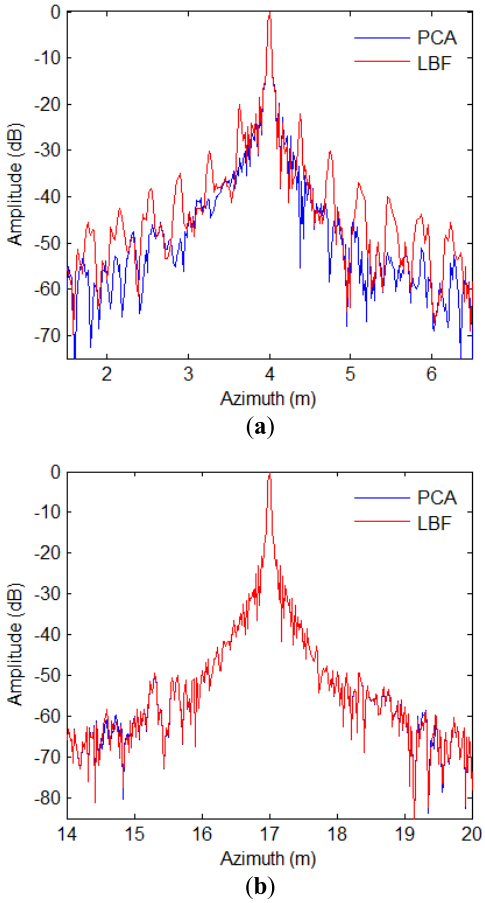

FIGURE 11. Azimuth slices for high frequency SAS. (a) close range; (b) far range.

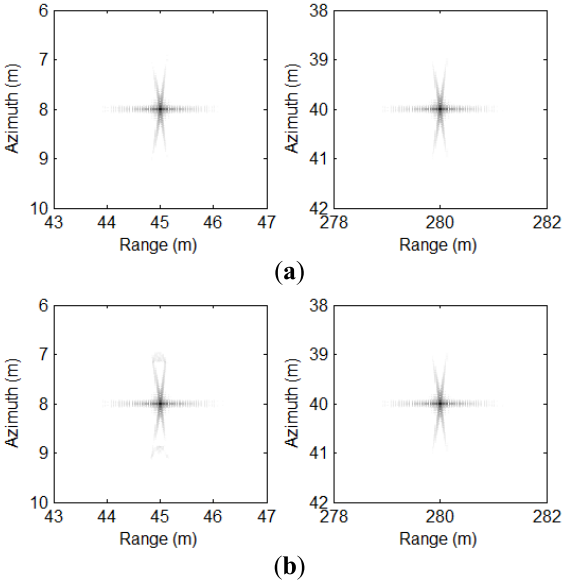

FIGURE 12. Imaging results of PCA method for low frequency SAS. (a) PCA method; (b) LBF method.

C. EXPERIMENTS WITH TRIAL DATA

In this section, the experiments with trial data are performed to further compare PCA and LBF methods. Fig.14 is the imagery results of LBF method. Fig. 14(a) is the result of a single blockwise and Fig.14(b) is the result of ten blockwises. Furthermore, the close look of enclosed area in Fig. 14(a) and Fig. 14(b) is presented in the right. The imagery result is enhanced by using ten blockwises compared to the single blockwise case. When the PCA method is used, the result is shown in Fig. 15. Comparing Fig. 14 and Fig. 15, we find that the PCA method can obtain much more optimum image compared to LBF method with fewer blockwises. When many blockwises are employed by LBF method, it can get high quality performance.

Fig. 16 further displays the azimuth slices of enclosed targets in Fig. 14 and Fig. 15. From this result, the LBF method needs much more blockwises to generate high resolution result which is similar to the result of PCA method. This conclusion is consistent with that from Fig. 14 and Fig. 15.

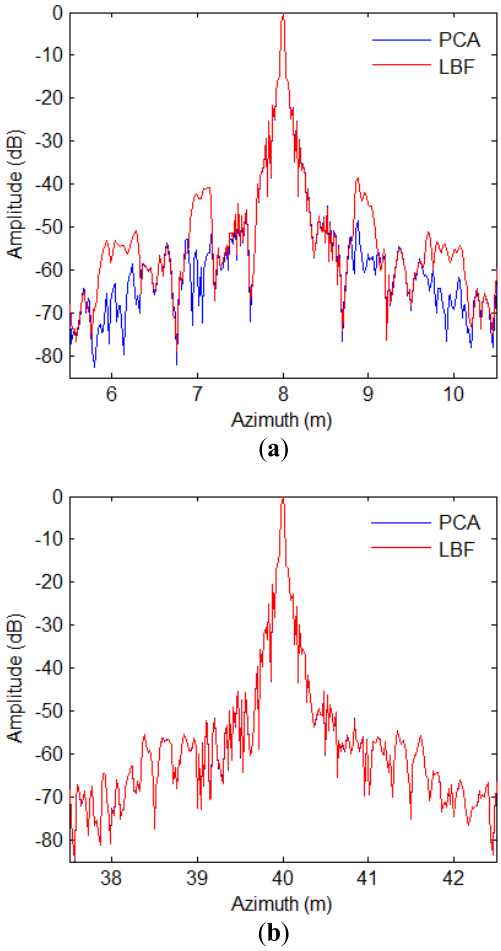

FIGURE 13. Azimuth slices for low frequency SAS. (a) close range; (b) far range.

TABLE 4. Performance of low frequency system.

	Close target			Far target		
	PSLR(dB)	ISLR(dB)	AR(cm)	PSLR(dB)	ISLR(dB)	AR(cm)
PCA	-15.08	-11.04	4	-14.36	-10.74	4
LBF	-15.00	-10.68	4	-14.37	-10.74	4

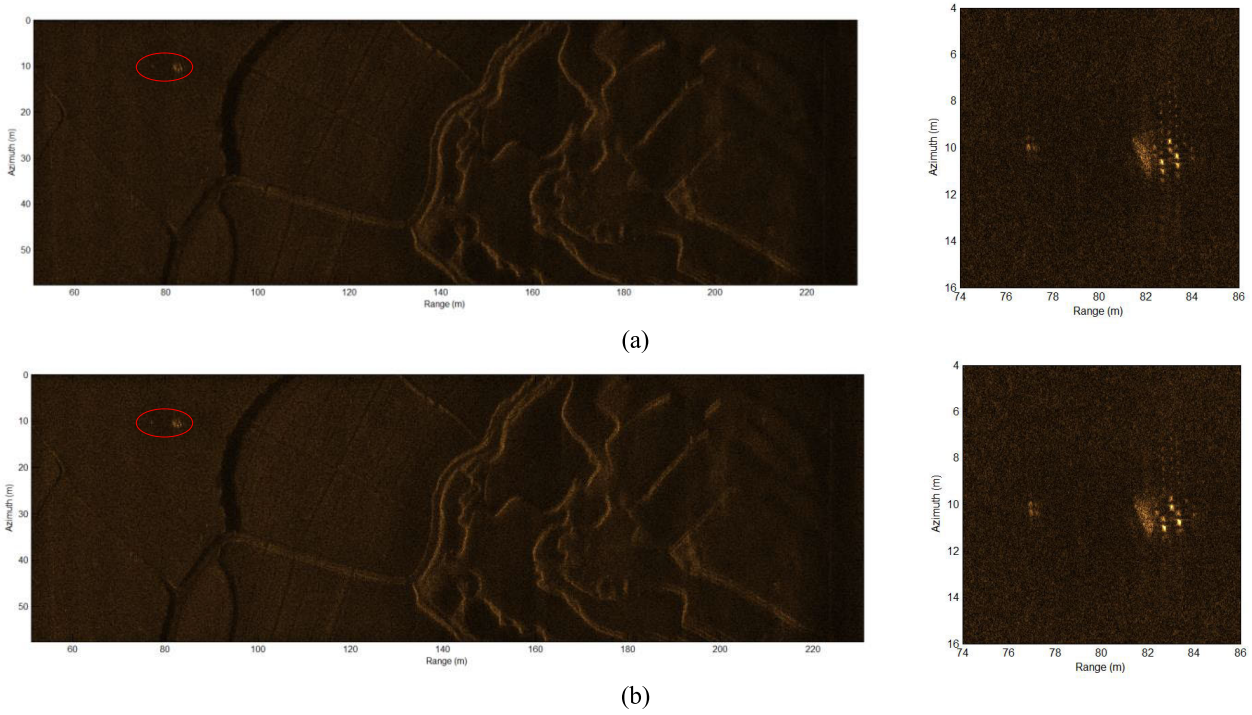

FIGURE 14. Experimental image with LBF. (a) single blockwise; (b) ten blockwises.

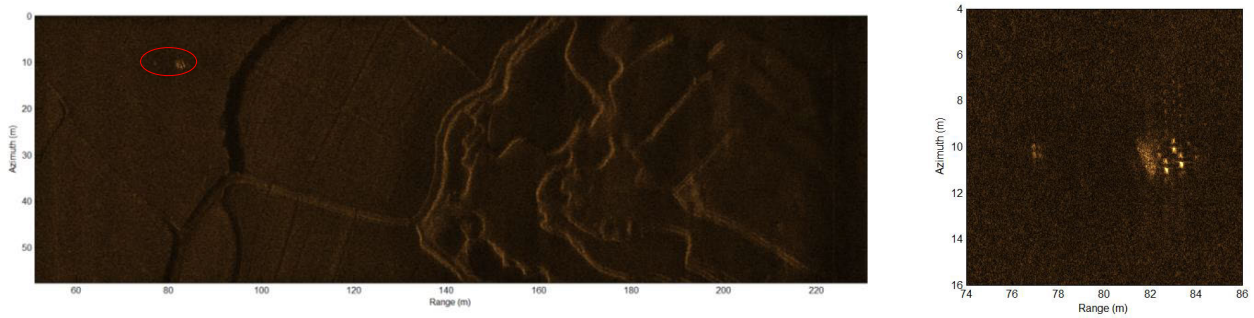

FIGURE 15. Experimental image with PCA.

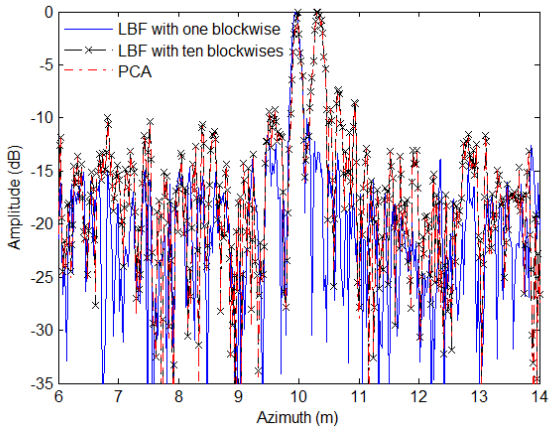

FIGURE 16. Azimuth slices of trial data.

Table 5 shows the processing time of LBF method and PCA method. The processing time of LBF method is slightly increasing with the blockwises, and the efficiency can be improved by about 7 times compared to PCA method.

TABLE 5. Processing time of trial data.

	LBF		PCA
	1 blockwise	10 blockwise	
Time (s)	126	223	1552

In general, the LBF and PCA methods are identical in theory. Since LBF suffers from actual phase error, the imaging capability of the PCA method outperforms that of the LBF technique. Because it is economical without interpolation, the LBF approach is more suited for long-range images.

VII. CONCLUSION

Imaging methods are crucial in multireceiver SAS systems. The multireceiver SAS imagery is a hard challenge. To use monostatic SAS imaging algorithms directly, the

multireceiver SAS datasets should first be produced into corresponding monostatic one. Currently, this transformation can be carried out by PCA method and LBF method, which are the approximation of accurate spectrum of multireceiver SAS system. Unfortunately, this transformation would lead to large approximation error, which is spatial-variance. It is hard to compensate the approximation phase error. In this paper, we comprehensively review the relationships between LBF and PCA methods, and obtain following conclusions:

1) The PCA and LBF methods are mostly identical in theory.

2) The LBF method would suffer from another phase error when the spectrum based on LBF is used to develop imaging algorithms. For PCA method, there is no other phase error.

3) The LBF is based on the quadratic expansion. At this point, the LBF would suffer from larger phase error than PCA method at close range. The phase errors based on both methods are mostly the same at far range. Due to this reason, the LBF is suited for far-target focusing.

4) The LBF is more effective than PCA methodology.

The LBF and PCA methods are just an approximation method to deduce the spectrum. The inaccuracy is introduced by approximation. When a narrow beam situation is occurred, the space variance of this error has a minor impact on reconstruction quality. However, the recover quality would be significantly degraded with wide beam case. Therefore, our current and future research is to correct the space-variant error generated by PCA and LBF approaches.

REFERENCES

[1] D. P. Williams, "On the use of tiny convolutional neural networks for human-expert-level classification performance in sonar imagery," *IEEE J. Ocean. Eng.*, vol. 46, no. 1, pp. 236–260, Jan. 2021.

[2] X. Zhang, J. Tang, and S. Zhang, "A chirp scaling algorithm for multi-receiver SAS imagery based on bistatic model," *Chin. High Technol. Lett.*, vol. 23, pp. 927–932, 2013.

[3] B. Thomas, A. Hunter, and S. Dugelay, "Phase wrap error correction by random sample consensus with application to synthetic aperture sonar micronavigation," *IEEE J. Ocean. Eng.*, vol. 46, no. 1, pp. 221–235, Jan. 2021.

[4] X. Zhang, P. Yang, P. Huang, H. Sun, and W. Ying, "Wide-bandwidth signal-based multireceiver SAS imagery using extended chirp scaling algorithm," *IET Radar, Sonar Navigat.*, vol. 16, no. 3, pp. 531–541, Mar. 2022.

[5] E. Moghimirad, C. A. V. Hoyos, A. Mahloojifar, B. M. Asl, and J. A. Jensen, "Synthetic aperture ultrasound Fourier beamformation using virtual sources," *IEEE Trans. Ultrason., Ferroelectr., Freq. Control*, vol. 63, no. 12, pp. 2018–2030, Dec. 2016.

[6] X. Zhang and P. Yang, "Back projection algorithm for multi-receiver synthetic aperture sonar based on two interpolators," *J. Mar. Sci. Eng.*, vol. 10, no. 6, p. 718, May 2022.

[7] C. Tan, X. Zhang, and P. Yang, "A novel sub-bottom profiler and signal processor," *Sensors*, vol. 19, no. 22, p. 5052, Nov. 2019.

[8] P. Huang and P. Yang, "Synthetic aperture imagery for high-resolution imaging sonar," *Frontiers Mar. Sci.*, vol. 9, Dec. 2022, Art. no. 1049761.

[9] X. Zhang, P. Yang, and M. Sun, "Experiment results of a novel sub-bottom profiler using synthetic aperture technique," *Current Sci.*, vol. 122, no. 4, pp. 461–464, 2022.

[10] S.-M. Steele, R. Charron, J. Dillon, and D. Shea, "Shallow water survey with a miniature synthetic aperture sonar," in *Proc. OCEANS MTS/IEEE SEATTLE*, Oct. 2019, pp. 1–6.

[11] X. Zhang, C. Tan, and W. Ying, "An imaging algorithm for multireceiver synthetic aperture sonar," *Remote Sens.*, vol. 11, no. 6, p. 672, Mar. 2019.

[12] M. Pinto, *300 kHz Interferometric Synthetic Aperture Sonar for High Performance Seabed Survey*. Oslo, Norway: AIP, 2013.

[13] P. Huang, X. Teng, and H. Zhong, "Adaptive filtering method combined with quality map for InSAS interferogram," *Electron. Lett.*, vol. 58, pp. 1009–1022, Dec. 2022.

[14] P. Huang, J. Tang, and H. Zhong, "Piecewise surface fitting method for complex image registration of interferometric synthetic aperture sonar," *Geomatics Inf. Sci. Wuhan Univ.*, vol. 46, pp. 1259–1264, Aug. 2021.

[15] P. Huang, J. Tang, H. Zhong, and K. Xu, "A new InSAS regestration method based on rational function surface fitting," *Geomatics Inf. Sci. Wuhan Univ.*, vol. 44, no. 4, pp. 601–607, 2019.

[16] A. Bellettini and M. Pinto, "Design and experimental results of a 300-kHz synthetic aperture sonar optimized for shallow-water operations," *IEEE J. Ocean. Eng.*, vol. 34, no. 3, pp. 285–293, Jul. 2009.

[17] J. J. Hall, M. R. Azimi-Sadjadi, S. G. Kargl, Y. Zhao, and K. L. Williams, "Underwater unexploded ordnance (UXO) classification using a matched subspace classifier with adaptive dictionaries," *IEEE J. Ocean. Eng.*, vol. 44, no. 3, pp. 739–752, Jul. 2019.

[18] X. Zhang, X. Dai, and B. Yang, "Fast imaging algorithm for the multiple receiver synthetic aperture sonars," *IET Radar, Sonar Navigat.*, vol. 12, no. 11, pp. 1276–1284, Nov. 2018.

[19] T. Berthomier, D. P. Williams, and S. Dugelay, "Target localization in synthetic aperture sonar imagery using convolutional neural networks," in *Proc. OCEANS MTS/IEEE SEATTLE*, Oct. 2019, pp. 1–9.

[20] T. G-Michael, J. Abiva, and R. G. Roberts, "Automated change detection: Applications for synthetic aperture sonar and future capabilities," *IEEE Syst. Man, Cybern. Mag.*, vol. 5, no. 3, pp. 60–C3, Jul. 2019.

[21] M. A. Pinto, A. Bellettini, R. Hollett, and A. Tesei, "Real- and synthetic-array signal processing of buried targets," *IEEE J. Ocean. Eng.*, vol. 27, no. 3, pp. 484–494, Jul. 2002.

[22] R. Bamler, "A comparison of range-Doppler and wavenumber domain SAR focusing algrorithms," *IEEE Trans. Geosci. Remote Sens.*, vol. 30, no. 4, pp. 706–713, Jul. 1992.

[23] X. Wang, X. Zhang, and S. Zhu, "Upsampling based back projection imaging algorithm for multi-receiver synthetic aperture sonar," in *Proc. Int. Ind. Informat. Comput. Eng. Conf.*, Jan. 2015, pp. 1610–1615.

[24] P. Yang and J. Liu, "Effect of non-unifrom sampling on sonar focusing," in *Proc. 14th Int. Conf. Commun. Softw. Netw. (ICCSN)*, Jun. 2022, pp. 109–113.

[25] H. J. Callow, M. P. Hayes, and P. T. Gough, "Advanced wavenumber domain processing for reconstruction of broad-beam multiple-receiver synthetic aperture imagery," in *Image and Vision Computing New Zealand*. Wellington, New Zealand: IVCNZ, 2001, pp. 51–56.

[26] X. Zhang, P. Yang, and M. Zhou, "Multireceiver SAS imagery with generalized PCA," *IEEE Geosci. Remote Sens. Lett.*, vol. 20, pp. 1–5, 2023.

[27] X. Zhang and P. Yang, "An improved imaging algorithm for multi-receiver SAS system with wide-bandwidth signal," *Remote Sens.*, vol. 13, no. 24, p. 5008, Dec. 2021.

[28] X. B. Zhang, J. S. Tang, H. P. Zhong, and S. Zhang, "Wavenumber-domain imaging algorithm for wide-beam multi-receiver synthetic aperture sonar," *J. Harbin Eng. Univ.*, vol. 35, no. 1, pp. 93–101, Jan. 2014.

[29] X. Wang and D.-Y. Zhu, "Range Doppler Algorithm for bistatic SAR processing based on the improved loffeld's bistatic formula," *Prog. Electromagn. Res. Lett.*, vol. 27, pp. 161–169, 2011.

[30] X. Zhang, P. Yang, X. Feng, and H. Sun, "Efficient imaging method for multireceiver SAS," *IET Radar, Sonar Navigat.*, vol. 16, no. 9, pp. 1470–1483, Sep. 2022.

[31] X. Zhang, H. Wu, H. Sun, and W. Ying, "Multireceiver SAS imagery based on monostatic conversion," *IEEE J. Sel. Topics Appl. Earth Observ. Remote Sens.*, vol. 14, pp. 10835–10853, 2021.

[32] X. Zhang and P. Yang, "Imaging algorithm for multireceiver synthetic aperture sonar," *J. Electr. Eng. Technol.*, vol. 14, no. 1, pp. 471–478, Jan. 2019.

[33] X. Zhang, X. Dai, and B. Fang, "A range-Doppler imaging method for the multireceiver synthetic aperture sonar," *Geomatics Inf. Sci. Wuhan Univ.*, vol. 44, no. 11, pp. 1667–1673, Nov. 2019.

[34] X. Zhang, J. Tang, S. Zhang, and H. Zhong, "Chirp-scaling imaging algorithm for multi-receiver synthetic aperture sonar," *Syst. Eng. Electron.*, vol. 35, pp. 1415–1420, Jul. 2013.

[35] P. T. Gough and M. P. Hayes, "Fast Fourier techniques for SAS imagery," in *Proc. MTS/IEEE Oceans Conf.*, Jun. 2005, pp. 563–568.

[36] X. Zhang, Y. Liu, and X. Deng, "Influence of phase centre approximation error on SAS imagery," in *Proc. IEEE 6th Int. Conf. Comput. Commun. Syst. (ICCCS)*, Apr. 2021, pp. 352–356.
[37] P. T. Gough, M. P. Hayes, and D. R. Wilkinson, "An efficient image reconstruction algorithm for a muliple hydrophone array synthetic aperture sonar," in *Proc. 5th Eur. Conf. Underwater Acoust. (ECUA)*, Jul. 2000, pp. 395–400.
[38] X. Zhang and C. Tan, "A comparison of PCA based imaging methods for the multireceiver SAS," in *Proc. IEEE 18th Int. Conf. Commun. Technol. (ICCT)*, Oct. 2018, pp. 946–950.
[39] A. Bellettini and M. A. Pinto, "Theoretical accuracy of synthetic aperture sonar micronavigation using a displaced phase-center antenna," *IEEE J. Ocean. Eng.*, vol. 27, no. 4, pp. 780–789, Oct. 2002.
[40] W. W. J. Bonifant, *Interferometric Synthetic Aperture Sonar Processing*. Atlanta, GA, USA: Georgia Institure of Technology, 1999.
[41] Z. Xu and K.-S. Chen, "Effects of the 'stop-and-go' approximation on the lunar-based SAR imaging," *IEEE Geosci. Remote Sens. Lett.*, vol. 19, pp. 1–5, 2022.
[42] X. Zhang, X. Chen, and W. Qu, "Influence of the stop-and-hop assumption on synthetic aperture sonar imagery," in *Proc. IEEE 17th Int. Conf. Commun. Technol. (ICCT)*, Oct. 2017, pp. 1601–1607.
[43] W. W. Bonifant, M. A. Richards, and J. H. McClellan, "Interferometric height estimation of the seafloor via synthetic aperture sonar in the presence of motion errors," *IEE Proc.-Radar, Sonar Navigat.*, vol. 147, no. 6, pp. 322–330, Dec. 2000.
[44] H. Yang, "Studies on imaging algorithm of multiple-receiver synthetic aperture sonar," Ph.D. dissertation, School Electron. Eng., Naval Univ. Eng., Wuhan, China, 2009.
[45] R. Wang, O. Loffeld, H. Nies, Q. Ul-Ann, A. M. Ortiz, and S. Knedlik, "A two-step method to process bistatic SAR data in the general configuration," in *Proc. IEEE Radar Conf.*, May 2008, pp. 1–5.
[46] K. Natroshvili, O. Loffeld, H. Nies, A. M. Ortiz, and S. Knedlik, "Focusing of general bistatic SAR configuration data with 2-D inverse scaled FFT," *IEEE Trans. Geosci. Remote Sens.*, vol. 44, no. 10, pp. 2718–2727, Oct. 2006.
[47] R. Wang, O. Loffeld, Q. Ul-Ann, H. Nies, A. M. Ortiz, and A. Samarah, "A bistatic point target reference spectrum for general bistatic SAR processing," *IEEE Geosci. Remote Sens. Lett.*, vol. 5, no. 3, pp. 517–521, Jul. 2008.
[48] P. Yang, "An imaging algorithm for high-resolution imaging sonar system," *Multimedia Tools Appl.*, vol. 2023, pp. 1–17, Sep. 2023, doi: 10.1007/s11042-023-16757-0.
[49] X. Zhang, P. Yang, and X. Dai, "Focusing multireceiver SAS data based on the fourth-order legendre expansion," *Circuits, Syst., Signal Process.*, vol. 38, no. 6, pp. 2607–2629, Jun. 2019.
[50] O. Loffeld, H. Nies, V. Peters, and S. Knedlik, "Models and useful relations for bistatic SAR processing," *IEEE Trans. Geosci. Remote Sens.*, vol. 42, no. 10, pp. 2031–2038, Oct. 2004.
[51] H. Nies, O. Loffeld, and K. Natroshvili, "Analysis and focusing of bistatic airborne SAR data," *IEEE Trans. Geosci. Remote Sens.*, vol. 45, no. 11, pp. 3342–3349, Nov. 2007.
[52] R. Wang, O. Loffeld, H. Nies, S. Knedlik, and J. H. G. Ender, "Chirp-scaling algorithm for bistatic SAR data in the constant-offset configuration," *IEEE Trans. Geosci. Remote Sens.*, vol. 47, no. 3, pp. 952–964, Mar. 2009.
[53] X. Zhang and W. Ying, "Influence of the element beam pattern on synthetic aperture sonar imaging," *Geomatics Inf. Sci. Wuhan Univ.*, vol. 47, no. 1, pp. 133–140, Jan. 2022.
[54] H. Pan and Z. Heping, "A raw echo simulation method based on reference signal translation for InSAS," in *Proc. 14th Int. Congr. Image Signal Process., Biomed. Eng. Informat. (CISP-BMEI)*, Oct. 2021, pp. 1–5.
[55] X. Zhang, "An efficient method for the simulation of multireceiver SAS raw signal," *Multimedia Tools Appl.*, vol. 2023, pp. 1–18, Sep. 2023, doi: 10.1007/s11042-023-16992-5.
[56] X. Zhang, W. Ying, and X. Dai, "High-resolution imaging for the multireceiver SAS," *The Jounal Eng.*, vol. 19, pp. 6032–6057, 2019.
[57] I. Cumming and F. Wong, *Digtal Processing of Synthetic Aperture Radar Data: Algorithms and Implementation*. Norwood, MA, USA: Artech House, 2005.
[58] X. Zhang, P. Yang, and H. Sun, "An Omega-k algorithm for multireceiver synthetic aperture sonar," *Electron. Lett.*, vol. 59, no. 13, pp. 1–3, Jul. 2023.
[59] J. Wu, W. Pu, Y. Huang, J. Yang, and H. Yang, "Bistatic forward-looking SAR focusing using w-k based on spectrum modeling and optimization," *IEEE J. Sel. Topics Appl. Earth Observ. Remote Sens.*, vol. 11, pp. 4500–4512, 2018.
[60] R. Wang, O. Loffeld, H. Nies, and J. H. G. Ender, "Focusing space-borne/airborne hybrid bistatic SAR data using wavenumber-domain algorithm," *IEEE Trans. Geosci. Remote Sens.*, vol. 47, no. 7, pp. 2275–2283, Jul. 2009.
[61] X. Zhang, W. Ying, Y. Liu, and X. Deng, "Processing multireceiver SAS data based on the PTRS linearization," in *Proc. IEEE Int. Geosci. Remote Sens. Symp. (IGARSS)*, Jul. 2021, pp. 5167–5170.
[62] B. Liu, T. Wang, Q. Wu, and Z. Bao, "Bistatic SAR data focusing using an Omega-K algorithm based on method of series reversion," *IEEE Trans. Geosci. Remote Sens.*, vol. 47, no. 8, pp. 2899–2912, Aug. 2009.

MENG WANG received the B.S. degree from the School of Computer Science, Liaocheng University, Liaocheng, China, in 2003, and the M.S. degree from the School of Information Science and Engineering, Shandong University of Science and Technology, China, in 2007. From 2003 to 2023, he was a Lecturer with the School of Mathematics and Information Science, Weifang University. His current research interests include parallel computing and the research and application of mathematical methods in image processing.

PAN HUANG (Member, IEEE) received the B.S. degree from the School of Mathematics and Information Science, Weifang University, Weifang, China, in 2009, the M.S. degree from the School of Science, Qingdao University of Technology, Qingdao, China, in 2012, and the Ph.D. degree from the Naval University of Engineering, Wuhan, China, in 2018. From 2018 to 2023, he was a Lecturer with the School of Mathematics and Information Science, Weifang University. His current research interests include the image processing of interferometric synthetic aperture sonar, partial differential equation theory, and its application in image processing.